Eur. Phys. J. B **13**, 227–233 (2000)

THE EUROPEAN PHYSICAL JOURNAL B

EDP Sciences

The Mössbauer and magnetic resonances investigations of structural phase transitions in K_2ZnCl_4 crystals

S. Constantinescu[a] and M.N. Grecu

National Institute for Materials Physics, 76900 Bucharest, Romania

Received 3 February 1999 and Received in final form 4 May 1999

Abstract. The experimental data carried out by Mössbauer and magnetic resonances investigations of the structural phase transitions in K_2ZnCl_4 crystals are discussed by a simple electrostatic model, calculating, the lattice contributions to the local electric potential $V(\mathbf{r})$, electric field intensity $\mathbf{E}(\mathbf{r})$ and electric field gradient tensor, $V_{\alpha\beta}(\mathbf{r})$ and taking into account both the fractional electric point charges and rigid lattice approximations. The validity of the model is proved by a good fit of the computing results and experimental data of quadrupole splitting parameters at K sites obtained by ^{39}K-NMR methods in high temperature incommensurate phase ($\sim$ Pnam *symmetry*). The experimental results obtained by Mössbauer and EPR methods in commensurate phase ($Pna2_1$ *symmetry*) of iron and copper doped K_2ZnCl_4 crystals are explained by relaxing the rigid lattice approximation. The insertion of probe ions appear to be done on not-exactly-Zn^{2+} site.

PACS. 76.80.+y Mössbauer effect; other γ-ray spectroscopy

1 Introduction

Like many other members of the A_2BX_4 family [1], K_2ZnCl_4 shows the following sequence of structural phase transitions. There is at $T_i = 553$ K a transition from normal paraelectric phase with the space group Pnam ($b > a > c$) and four molecules per unit cell to an incommensurate phase ($q/a^* = (1-\delta)/3$ with $\delta \ll 1$). At $T_c = 403$ K a lock-in transition to a commensurate ferroelctric phase ($q/a^* = 1/3$) with the space group $Pna2_1$ and 12 molecules per unit cell has evidenced. Also at $T_{c1} = 145$ K there is another phase transition to a monoclinic commensurate ferroelectric phase with the space group A11a and 48 molecules per unit cell.

Very recently, a second low-temperature incommensurate phase between 152 K and 145 K has reported [2,3]. Quilichini [3] revealed by inelastic neutron scattering a soft optic phonon with a wave vector $q = 0.5b^* + (0.5-\delta)c^*$, $\delta \ll 1$ responsible for this incommensurate phase transition. The structures and properties of some phases in K_2ZnCl_4 differ considerably from those of the prominent members of the A_2BX_4 family. The unusual feature is the presence, in the high temperature incommensurate phase, of large thermal hysteresis, memory effects and extremely slow relaxation of the dielectric constant [4].

In the present work the local electric potential, electric field intensity and static part of the lattice electric field gradient (efg) behaviours at K sites in Pnam phase of K_2ZnCl_4 are probed by numerical calculations. These calculations have been performed using fractional ionic point charges and rigid lattice approximations respectively. We have extended the model relaxing the last approximation and allowing hopping of the sites along the a axis and ferroelectric c axis. We have evaluated the local electric properties dependencies with the displacement along one direction from the nominal cation sites. The computing results have compared with the experimental data obtained by NMR, Mössbauer and EPR methods on iron and copper doped potassium tetrachlorozincate.

[a] e-mail: sconst@alpha1.infim.ro

2 Local electric properties computation

The lattice contribution to the local electric potential $V(\mathbf{r})$, intensity $\mathbf{E}(\mathbf{r})$ and $V(\mathbf{r})$ tensor at cation sites $\mathbf{r}_o(x_o, y_o, z_o)$ in the ferroelectric structure of K_2ZnCl_4 have been calculated by QSLATT3, a new version of the computing program QSCOMP [5]. The starting expressions are:

$$V(\mathbf{r}) = \frac{1}{4\pi\varepsilon_o} \int_r \frac{\rho(\mathbf{r}')}{|\mathbf{r}-\mathbf{r}_o|} \mathrm{d}\mathbf{r}'$$

$$\mathbf{E}(\mathbf{r}') = -\boldsymbol{\nabla} V(\mathbf{r}')$$

$$efg = V_{\alpha\beta}(\mathbf{r}) = -\boldsymbol{\nabla}\mathbf{E}(\mathbf{r}) = \boldsymbol{\nabla}(\boldsymbol{\nabla} V(\mathbf{r})) = \begin{vmatrix} V_{xx} & V_{xy} & V_{xz} \\ V_{xy} & V_{yy} & V_{yz} \\ V_{xz} & V_{yz} & V_{zz} \end{vmatrix} \quad (1)$$

where $\rho(\mathbf{r})$ is the lattice charge distribution around $\mathbf{r}_o$ and ε_o is the vacuum electric permitivity. The computing

procedure takes into account the point charge approximation of crystal field theory:

$$\rho(\mathbf{r}') = \sum_{i=1}^{N} q_i \delta(\mathbf{r}' - \mathbf{r}_i). \quad (2)$$

In this approximation the lattice contributions to the local electric properties in $\mathbf{r}_o$ are given by the relations:

$$V^{\text{latt}}(\mathbf{r}_o) = \frac{1}{4\pi\varepsilon_o} \sum_{i=1}^{N_i} \frac{q_i}{|\mathbf{r} - \mathbf{r}_o|}$$

$$\mathbf{E}^{\text{latt}}(\mathbf{r}_o) = \frac{1}{4\pi\varepsilon_o} \sum_{i=1}^{N_i} \frac{q_i (\mathbf{r}_i - \mathbf{r}_o)}{|\mathbf{r}_i - \mathbf{r}_o|^3}$$

$$V^{\text{latt}}_{\alpha\beta}(\mathbf{r}_o) = \frac{1}{4\pi\varepsilon_o} \sum_{i=1}^{N_i} \frac{q_i}{|\mathbf{r}_i - \mathbf{r}_o|^5} \Big[3(x_{i\alpha} - x_{o\alpha})(x_{i\beta} - x_{o\beta}) - |\mathbf{r}_i - \mathbf{r}_o|^2 \delta_{\alpha\beta}\Big]. \quad (3)$$

The positions $\mathbf{r}_i$ (and $d_i = |\mathbf{r}_i - \mathbf{r}_o|$) of the crystallographic cationic sites are given by the subroutine LATTICE according to the relation:

$$\mathbf{r}_i = (x_{io} + la)\,\mathbf{i} + (y_{io} + mb)\,\mathbf{j} + (z_{io} + nc)\,\mathbf{k} \quad (4)$$

where $\mathbf{r}_o(x_{io}, y_{io}, z_{io})$ designates the positions of the N_i^o charges q_i in the rectangular unit cell with the lattice constants a, b, c, $(i = 1, 2, \ldots N = (2l+1)(2m+1)(2n+1)N_i^o)$. The co-ordinates x_{io}, y_{io}, z_{io} and the lattice constants a, b, c for the studied structure are obtained from X-ray or neutron diffraction measurements. δ is the Kroneker's symbol. The values for charges q_i are given by the usual ionic charges or they can be obtained by other procedures, *e.g.* a valence summation, described recently in [7].

With the above mentioned quantities, the efg tensor components $V^{\text{latt}}_{\alpha\beta}(\mathbf{r}_o)$ are calculated by subroutine GRADIENT. The principal components V_{XX}, V_{YY}, V_{ZZ}, and the asymmetry parameter $(\eta = (V_{XX} - V_{YY})/V_{ZZ})$, the corresponding eigen vectors and the Euler angles (α, β, γ), between the efg tensor principal axes and the crystallographic axes, are obtained by the diagonalisation subroutine EIGEN.

The r^{-n} $(n = 1, 2, 3)$ dependencies of local electric properties are more important for the ions directly coordinated to the central ion, *i.e.* for ligands, than more distant ions in the lattice.

On the other hand a complete neglect of distant ions may led to inaccuracies of the computing data and their comparison to the experimental ones. The new version of QSCOMP allows to calculate the local electric properties both of the ligand and also of the different surrounding shells contribution and the rest of lattice one.

$$V^{\text{latt}}(\mathbf{r}_o) = V^{\text{lig}}(\mathbf{r}_o) + V^{\text{rest}}(\mathbf{r}_o)$$
$$\mathbf{E}^{\text{latt}}(\mathbf{r}_o) = \mathbf{E}^{\text{lig}}(\mathbf{r}_o) + \mathbf{E}^{\text{rest}}(\mathbf{r}_o)$$
$$V^{\text{latt}}_{\alpha\beta}(\mathbf{r}_o) = V^{\text{lig}}_{\alpha\beta}(\mathbf{r}_o) + V^{\text{rest}}_{\alpha\beta}(\mathbf{r}_o). \quad (5)$$

The dispersion of V, $\mathbf{E}$ and $V_{\alpha\beta}$ values related to the shifted cationic position in the lattice is given by:

$$V^{\text{latt}}(\mathbf{r}_o + \delta\mathbf{r}) = V^{\text{lig}}(\mathbf{r}_o) + \boldsymbol{\nabla} V^{\text{rest}}(\mathbf{r}_o) \cdot \delta\mathbf{r}$$
$$E^{\text{latt}}_{\alpha}(\mathbf{r}_o + \delta\mathbf{r}) = E^{\text{lig}}_{\alpha}(\mathbf{r}_o) + \boldsymbol{\nabla} E^{\text{rest}}_{\alpha}(\mathbf{r}_o) \cdot \delta\mathbf{r}$$
$$V^{\text{latt}}_{\alpha\beta}(\mathbf{r}_o + \delta\mathbf{r}) = V^{\text{lig}}_{\alpha\beta}(\mathbf{r}_o) + \boldsymbol{\nabla} V^{\text{rest}}_{\alpha\beta}(\mathbf{r}_o) \cdot \delta\mathbf{r}. \quad (6)$$

3 Experimental

The electric quadrupolar hyperfine interaction between the probe and the neighbourhood can be evidenced by the NMR, NQR, Mössbauer and EPR experimental methods. The principal efg tensor components V^{obs} can be evaluated from the spectra by the relations

$$V^{\text{obs}}_{ZZ} = \begin{cases} 4.1357 \times 10^{-15} \dfrac{2\varepsilon_Q^{\text{obs}}}{(1-\gamma_\infty) e Q_{^{39}\text{K}}} \\ \qquad \leftarrow \text{ NMR, NQR method} \\ 4.8038 \times 10^{-8} \dfrac{2\Delta E_Q^{\text{obs}}}{(1-\gamma_\infty) e Q_{^{57}\text{Fe}} \sqrt{1+\eta^2/3}} \\ \qquad \leftarrow \text{ Mössbauer method} \\ 1.1577 \times 10^{-8} \dfrac{P_{ZZ}^{\text{obs}}}{(1-\gamma_\infty) e Q_{^{63}\text{Cu}}} \\ \qquad \leftarrow \text{ EPR method} \end{cases} \quad (7)$$

where $\varepsilon_Q^{\text{obs}}$, ΔE_Q^{obs}, P_{ZZ}^{obs} are the spectral parameters of the mentioned experimental methods. Q is the nuclear quadrupole moment and γ_∞ is the Sternheimer factor. The Q and values used in the calculus were $Q(^{57}\text{Fe}) = 0.21 \times 10^{-28}$ m^2, $\gamma_\infty(^{57}\text{Fe}^{3+}) = -10.6$, $Q(^{63}\text{Cu}) = -0.15 \times 10^{-28}$ m^2, $\gamma_\infty(^{63}\text{Cu}^{2+}) = -25$, $Q(^{39}\text{K}) = 0.09 \times 10^{-28}$ m^2 and $\gamma_\infty(^{39}\text{K}^{+}) = -20$, [6,7]. The numerical coefficients are energy conversion factors between the specific to eV units. The principals components of efg tensor, $V^{\text{obs}}_{\alpha\alpha}$ in V/m^2, given in Table 1, have extracted by a refined analyse of spectral parameters of hyperfine electric quadrupole interaction from the ^{39}K-NMR spin-echo spectra recorded in a superconducting magnet at Larmor frequency of $\nu_L = 16.628$ MHz [13], from ^{57}Fe-Mössbauer spectra obtained in transmission geometry in the velocity range ± 3 mm/s using a ^{57}Co:Cu source (50 mCi) with $f = 0.73$ and $\Gamma_s = 0.11$ mm/s [12] and from EPR spectra carried out with a JES ME-3X spectrometer with 100 kHz modulation [14], for pure and iron and copper doped K_2ZnCl_4 crystals. The temperature instability over the measuring period was less than 0.5 K.

The $V^{\text{obs}}_{\alpha\alpha}$ values are compared with the V^{latt} obtained from computing results taking into account the proposed model.

4 Computation results and discussions

4.1 Calculation of $V_{\alpha\beta}(r)$ on cation sites

The numerical computation of the lattice efg tensor at cation sites in K_2ZnCl_4 has been performed according to

Table 1. Experimental values of the spectral parameters in specific units.

Experimental method	T [K]	Spectral parameters of quadrupole splitting interaction	$V_{ZZ}^{\rm obs}$ $[10^{20}\frac{\rm V}{\rm m^2}]$
^{39}K-NMR	∼550	$2\varepsilon_Q'^{\rm obs} = 0.437$ MHz; $\eta = 0.13$ [13]	2.001(3)
^{57}Fe-Mössbauer effect	296	$\Delta E_Q^{\rm obs} = 0.306(6)$ mm/s [12]	1.273(12)
Cu^{2+}-EPR	290	$P_{zz}^{\rm obs} = -12.4(5)$ G	3.6(1)
		$P_{xx}^{\rm obs} = 6.9(5)$ G [14]	−2.0(1)
		$P_{yy}^{\rm obs} = 5.5(5)$ G	−1.6(1)

the procedure described in the above section. The lattice of rectangular unit cell was built by the subroutine LATTICE with the origin of coordinates in the crystallographic position 4a for the normal (paraelectric), incommensurate and commensurate (ferroelectric) phases. There are two and six different K positions and one and three different Zn positions in the paraelectric and respectively ferroelectric unit cell. The principal components of the efg tensor were provided by subroutine GRADIENT, taking into account the LATTICE output data for $N = 756$ and 2268 ions situated at their crystalline sites, *i.e.* contained within a radius of 26 unit cells.

Table 2 is showing the fractional positions [3,9], and electric point charges, obtained by the valence summation procedure, described in [7], in the normal, $N(b > a > c)$ incommensurate, INC and commensurate, C phases. The fractional electric point charges of K_2ZnCl_4 structure are $q_i = \sum_{\alpha=1}^{N_i} v_\alpha^i$, where v_α^i and N_i are the valence bond and the number of the nearest ions of q_i charge respectively. The electric charges are given in electron charge units.

The authors performed a numerical calculus of the local electric properties, $V(\mathbf{r})$, $\mathbf{E}(\mathbf{r})$ and $V_{\alpha\beta}(\mathbf{r})$ at cation sites in C ($Pna2_1$-symmetry) and INC (∼ Pnam-symmetry, model 1 [3]) phases in order to compare them with NMR, Mössbauer and EPR experimental data obtained at the high temperature part of INC phase [13] and respectively at 296 K and 290 K, corresponding to C phase [12,14]. As one can see from Figure 1, the convergence of the lattice sum contribution to $V_{ZZ}^{\rm latt}$ as function of radius d for a given coordination sphere is practically obtained for 7 Å.

Table 3 sums up the computed data V, V_{ZZ} and η obtained at Zn and K sites of K_2ZnCl_4, in the above mentioned phases for the ligand contribution ($V^{\rm lig}$, $V_{ZZ}^{\rm lig}$ and $\eta^{\rm lig}$) and all 2268 neighbours ($V^{\rm latt}$, $V_{ZZ}^{\rm latt}$ and $\eta^{\rm latt}$) taking into account the ionic point charges.

We considered of interest to calculate the relative deviation between the computing and experimental data using the relation $R = |1 - V^{\rm obs}/V_{\rm calc}|$.

The R values, shown in Table 3, have evidenced a notable difference between $V^{\rm obs}$ and $V^{\rm latt}$ values ($1 \leq R^{\rm latt} \leq 10$), for all considered experimental data. That one can explain by the presence of a slow spatial dependence of Sterheimer factors. $V^{\rm lig}$ values are more closed for experimental Mössbauer and EPR data $V^{\rm obs}$, but the

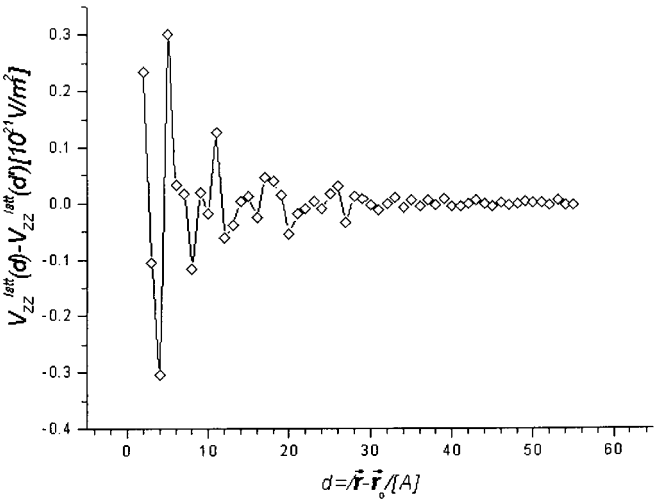

Fig. 1. The convergence of $V_{ZZ}^{\rm latt}$ with respect of radius of coordination sphere.

nearest are for NMR ones, ($R_{\rm NMR}^{\rm lig} < R_{\rm Moss}^{\rm lig}$, $R_{\rm EPR}^{\rm lig}$). On the other hand the $R_{\rm K-NMR}^{\rm lig}$ values in INC phase are showing that the point charge approximation model is not so far from a realistic one. In order to improve the agreement between $V^{\rm obs}$ and $V^{\rm calc}$, the authors taken into account an fractional ionic point charge approximation for the rigid crystal lattice.

The principal efg tensor components at K sites, calculated for lattice contributions taking into account both the nearest and all 2268 neighbours, are given in Table 4. As it can be seen from the table, the computing values of $V_{ZZ}^{\rm lig}$, obtained in the fractional ionic charge and rigid lattice approximations, are closely related to the experimental NMR quadrupole splitting constant reported in the reference [13], that means the well-known value $\gamma_\infty(^{39}K^+) = -20$ given in [6] corresponds to the next nearest neighbours. This concordance for $^{39}K_2ZnCl_4$ in INC phase, show the consistency of the approximations used to describe the local electric properties in such kind of crystals.

The comparison between R values obtained in the ionic (see Tab. 3) and fractional ionic point charges (see Tab. 5) has shown a narrowing tendency of their field, but perfectible especially for $^{63}Cu^{2+}$. In order to obtain a good fitness between the experimental and computing data one can relax the rigid lattice approximation.

Table 2. The fractional position [3,9] and fractional point charges of ions in the N paraelectric, INC and C ferroelectric phases of K_2ZnCl_4 obtained like as in [7].

Site	x^o/a	y^o/b	z^o/c	q[/e/]
N* Pnam phase				
K1	0.6354(15)	0.4114(12)	0.7500	1.1064(2)
K2	0.4942(10)	0.8129(6)	0.7500	1.0172(2)
Zn	0.2195(4)	0.4205(4)	0.7500	2.0004(2)
Cl_1	0.9768(4)	0.4288(4)	0.2500	−1.0512(2)
Cl_2	0.3231(4)	0.5797(4)	0.2500	−1.0715(2)
Cl_3	0.3063(4)	0.3368(6)	0.0055(5)	−0.9880(2)
Cl_4	0.3202(17)	0.3368(17)	0.0055(5)	−1.−133(2)
INC** Model 1				
K1	0.6339(16)	0.4143(18)	0.2500	1.219(2)
K2	0.4960(13)	0.8126(9)	0.2500	1.000(2)
Zn	0.2190(6)	0.4188(5)	0.2500	2.000(2)
Cl_1	0.9748(6)	0.4342(5)	0.2500	−1.160(2)
Cl_2	0.3309(6)	0.5782(2)	0.2500	−1.097(2)
Cl_3	0.3028(7)	0.3325(6)	0.0055(7)	−0.983(2)
Cl_4	0.3028(7)	0.3325(6)	0.5058(10)	−0.983(2)
C*** $Pn2_1$ phase				
K1	0.0433(1)	0.0814(4)	0.7866(9)	1.235(3)
K2	0.3797(1)	0.0855(5)	0.7638(9)	1.152(3)
K3	0.7106(1)	0.0833(4)	0.7223(7)	1.023(3)
K4	0.3319(1)	0.6875(3)	0.7219(6)	1.028(3)
K5	0.6660(1)	0.6863(3)	0.7388(6)	1.037(3)
K6	0.9986(1)	0.6883(3)	0.7932(6)	1.011(3)
Zn1	0.0721(1)	0.4194(1)	0.75000	2.000(3)
Zn2	0.4050(1)	0.4181(1)	0.7796(2)	2.000(3)
Zn3	0.7403(1)	0.4177(1)	0.7365(2)	2.004(3)
Cl_1	0.9917(1)	0.4337(3)	0.6731(6)	−1.267(3)
Cl_2	0.1123(1)	0.5756(3)	0.8151(7)	−0.987(3)
Cl_3	0.0844(1)	0.3012(3)	0.9795(6)	−1.099(3)
Cl_4	0.1111(1)	0.4366(3)	0.4910(6)	−1.055(3)
Cl_5	0.3229(1)	0.5782(4)	0.8129(7)	−0.990(3)
Cl_6	0.4439(2)	0.3072(5)	0.8132(9)	−0.969(3)
Cl_7	0.4353(2)	0.3480(4)	−0.0004(7)	−0.787(3)
Cl_8	0.4306(2)	0.4358(3)	0.5110(6)	−0.900(3)
Cl_9	0.6591(1)	0.5760(4)	0.8044(7)	−1.355(3)
Cl_{10}	0.7794(1)	0.3615(3)	0.6660(8)	−0.948(3)
Cl_{11}	0.7778(1)	0.2942(3)	−0.0026(6)	−1.126(3)
Cl_{12}	0.7560(1)	0.2942(3)	0.5177(6)	−1.003(3)

*a = 8.926 Å; b = 12.402 Å; c = 7.256 Å; **a = 8.96 Å; b = 12.54 Å; c = 7.30 Å; ***a = 26.778 Å; b = 12.402 Å; c = 7.256 Å.

Table 3. The numerical values of $V_{ZZ}^{\rm lig}$, $\eta^{\rm lig}$, $V_{ZZ}^{\rm latt}$, $\eta^{\rm latt}$ and R at K and Zn sites, calculated in the ionic point charge approximation.

Cationic site	V [V]	V_{ZZ} [$10^{20}\frac{\rm V}{\rm m^2}$]	η	R ^{39}K	^{59}Fe	^{63}Cu
INC Model 1						
$K1^{+}$	−24.75	1.5041	0.83	0.3302		
$^{++}$	−5.67	−0.1924	0.71	9.3992		
$K2^{+}$	−31.24	1.2619	0.38	0.5487		
$^{++}$	−7.14	−0.7278	0.85	1.7491		
$Pna2_1$ phase						
$Zn1^{+}$	−25.47	0.536	0.74		1.3371	5.6427
$^{++}$	−15.11	−0.370	0.87		2.4397	7.1838
$Zn2^{+}$	−25.66	−0.553	0.27		1.3014	5.4385
$^{++}$	−14.97	−0.366	0.21		2.7878	8.7281
$Zn3^{+}$	−25.44	0.541	0.75		1.3525	5.5813
$^{++}$	−15.24	0.386	0.91		2.2972	8.2241

$^{+}$ Ligand contributions; $^{++}$26 neighbors cells contributions.

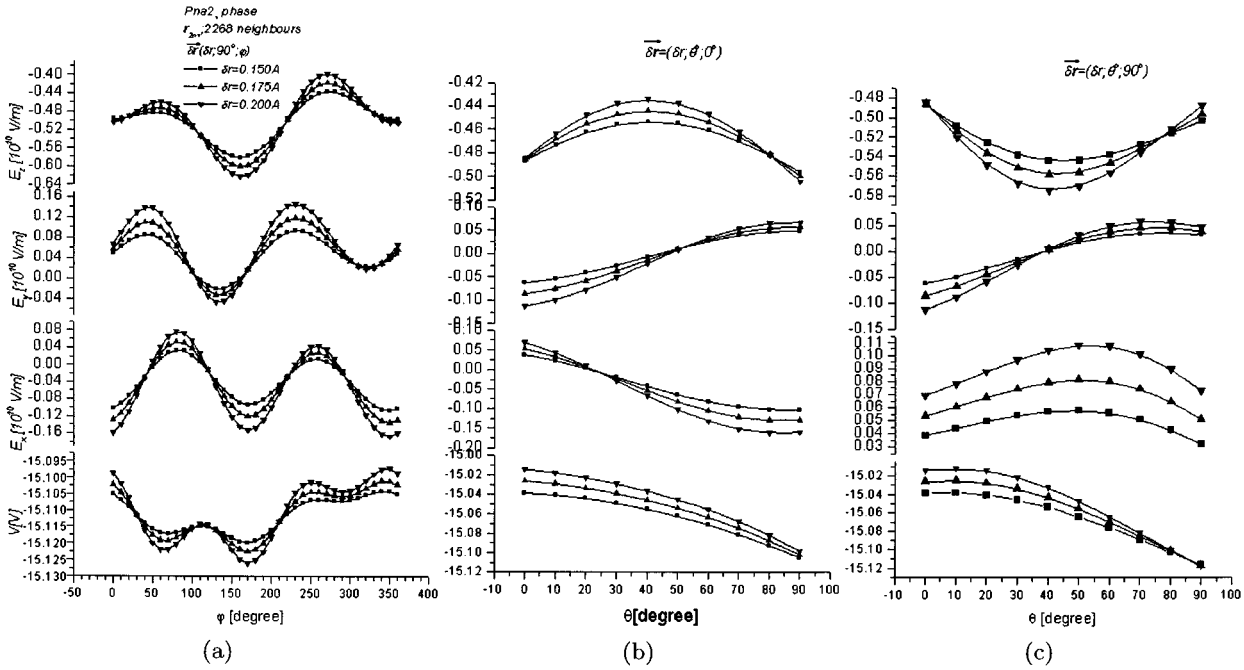

Fig. 2. The dependences of the local electric properties $V(\mathbf{r})$, $\mathbf{E}(\mathbf{r})$ relative to $\delta\mathbf{r} = \mathbf{r} - \mathbf{r}_{\rm Zn1}$ in different crystallographic planes in $Pna2_1$ phase.

Table 4. The numerical values of V_{ZZ}, and R at K sites, calculated in the ionic fractional charge approximation for incommensurate phase.

Site	V [V]	V_{ZZ} [$10^{20}\frac{\rm V}{\rm m^2}$]	η	R
INC Model 1				
K1 +	−27.52	1.6840	0.75	0.1870
++	−6.05	0.4028	0.96	3.9672
K2 +	−31.95	1.5729	0.24	0.2720
++	−6.09	0.8413	0.09	1.3782

Table 5. The numerical values of $V_{ZZ}^{\rm lig}$, $\eta^{\rm lig}$, $V_{ZZ}^{\rm latt}$ and $\eta^{\rm latt}$ at Zn sites, calculated in the fractional ionic point charge and rigid lattice approximations.

Cationic site	V	V_{ZZ} [V]	η [$10^{20}\frac{\rm V}{\rm m^2}$]	R ^{59}Fe	^{63}Cu
$Pna2_1$ phase					
Zn1 +	−28.091	−1.0175	0.72	0.2157	2.4988
++	−16.564	−0.8916	0.75	0.4278	2.9928
Zn2 +	−23.398	−0.7717	0.92	0.6496	3.6132
++	−12.786	−0.5343	0.89	1.3826	5.6629
Zn3 +	−28.212	−1.2016	0.43	0.0594	1.9627
++	−15.021	−0.8375	0.59	0.5200	0.2507

4.2 Calculations of V(r), E(r) and $V_{\alpha\beta}$(r) taking into account metallic cation displacements

To establish the real site of the iron and copper probes in the lattice an effective-field model [10] has been developed. In the first step, the position of the probe was gradually shifted from the cation site with $\delta\mathbf{r}(\delta r, \vartheta, \varphi) = \mathbf{r} - \mathbf{r}_{\rm Zn}$ and $V(\mathbf{r})$, $\mathbf{E}(\mathbf{r})$, $V_{\alpha\beta}(\mathbf{r})$-tensor components were

Table 6. (a) The numerical values of $V(\mathbf{r})$, $V_{ZZ}^{\rm lig}$, η, Euler angles and R ratio, calculated in the fractional charge approximation at ^{59}Fe in shifted Zn positions. (b) The numerical values of $V(\mathbf{r})$, $V_{ZZ}^{\rm lig}$, η, Euler angles and R ratio in the ionic fractional charge approximation at shifted Zn 1 positions for $^{63}Cu^{2+}$ probe.

(a)

Cation site	$\lvert\delta\mathbf{r}\rvert$ [Å]	V [V]	ϑ [°]	φ [°]	V_{ZZ} [$10^{20}\frac{\rm V}{\rm m^2}$]	η	α [°]	β [°]	γ [°]	R
Zn1 +	0.13	−28.14	170	222	−1.2427	0.72	−90	−90	−90	0.024
++	0.12	−16.35	156	131	−1.2064	0.92	−90	−90	−90	0.055
Zn2 +	0.13	−23.44	90	60	1.0967	0.95	0	57	−90	0.161
++	0.14	−12.93	140	130	1.2895	0.60	0	48	−90	0.013
Zn3 +	0.14	−28.30	23	332	1.2485	0.77	90	−90	−63	0.020
++	0.13	−15.05	188	9	−1.1937	0.96	0	−90	−90	0.067

(b)

	0.25	−28.22	90	180	−3.3097	0.72	−90	−90	−90	0.075
	0.30	−28.30	230	0	−3.4466	0.92	−90	−90	−90	0.033
	0.45	−28.27	190	90	−3.4609	0.95	−90	−90	−90	0.29

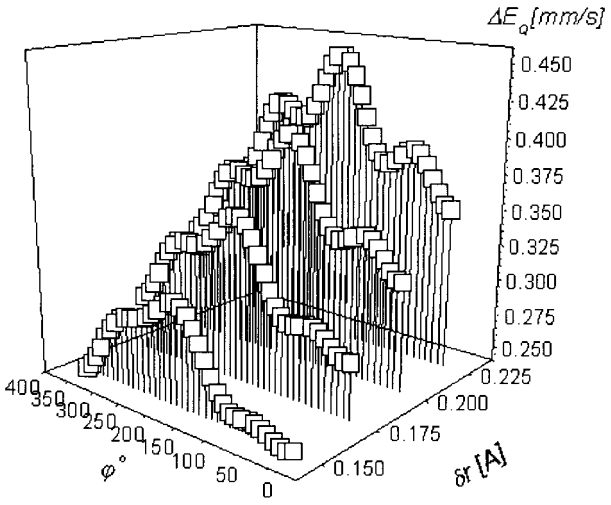

Fig. 3. The quadrupole splitting $\Delta E_{\rm Q}$ dependence on $\delta\mathbf{r} = \mathbf{r} - \mathbf{r}_{\rm Zn1}$ in the ab plane in $Pna2_1$ phase of ^{57}Fe:K_2ZnCl_4.

calculated. All ionic point charges have usual ionic charge values. The dependencies on $\delta\mathbf{r}$, of the local electrical properties at Zn1 site corresponding to $Pna2_1$ phases are shown in the Figure 2. As we can see the local electric properties $V(\delta\mathbf{r})$, $E_x(\delta\mathbf{r})$, $E_y(\delta\mathbf{r})$, $E_z(\delta\mathbf{r})$ are oscillating functions relative to polar angles. One can point out the differences of the local electric properties' dependencies in the crystallographic planes containing c-axis. The dependence of the quadrupole splitting parameter $\Delta E_{\rm Q}$, on $\delta\mathbf{r}$ are plotted in Figure 3 for (ab) plane in the $Pna2_1$ phase. The $\Delta E_{\rm Q}$ parameter generally shows an increasing dependence on $\delta\mathbf{r}$ and the maximum $\Delta E_{\rm Q}$ values are reached along a-axis, $\varphi = (180^{\rm o} \div 190^{\rm o})$. For these values the principal V_{ZZ} axis is along b one and asymmetry parameter is in the range $\eta \in (0.25 \div 0.50)$. In order to determine all the $\delta\mathbf{r}$ positions corresponding to $\Delta E_{\rm Q}^{\rm obs}$ for ^{57}Fe and to $P_{ZZ}^{\rm obs}$ for ^{63}Cu, the QSLATT3 program swept step by step ($\Delta\delta r = 0.025$ Å, $\Delta\varphi$, $\Delta\vartheta = 10^{\rm o}$) the whole space around the cation sites taking into account the fractional ionic charges determined by the valence summation procedure.

The founded positions $\delta\mathbf{r}(\delta x, \delta y, \delta z)$ are selected by the criteria of the minimum of electrostatic energy, $qV(\mathbf{r})$ of iron and copper probes. The most closed computed values, $V_{ZZ}^{\rm calc}$ to $V_{ZZ}^{\rm obs}$ (^{57}Fe and ^{63}Cu) obtained in the fractional ionic approximation for shifted Zn positions are given in Tables 6a and respectively 6b.

As one can observe from the R values the ^{57}Fe Mössbauer and Cu^{2+} EPR experimental data could be explained by the location of the probes in the Zn sites shifted with $|\delta\mathbf{r}| = 0.15$, 0.30 Å for iron and copper probe respectively. It was difficult to distinguish between the equivalent Zn sites in the commensurate phase due to small differences, $V(\mathbf{r}_{{\rm Zn}i}) - V(\mathbf{r}_{{\rm Zn}j})$. The authors suggest that the difference of the $|\delta\mathbf{r}|$ values for iron and copper ions could be explained by the different ionic radii and electronegativities.

5 Summary

The electrostatic model computation of the local electric properties at cation sites in the in- and commensurate phases of K_2ZnCl_4 was developed. The relative deviation between the experimental and computing results, R values, provides a rather good agreement with the magnetic resonances and Mössbauer data, by taking into account the ionic fractional charge approximation. The computed ^{39}K efg values incommensurate phases fit well with the NMR data [13]. Consequently we conclude that the fractional ionic point charge model is an acceptable model to calculate the local electric properties in the structural phase transitions of K_2ZnCl_4. Moreover the location of the 3d impurities (Cu and Fe) have been determined by relaxing the rigid lattice approximation. Off-centre Zn sites for the impurity probes in the crystal were proposed in order to explain the experimental EPR and Mössbauer data carried out in the iron and copper doped K_2ZnCl_4 crystals.

References

1. H.Z. Cummins, Phys. Rept. **185**, 211 (1990).
2. M.N. Grecu, P. Cevc, R. Blinc, Solid State Commun. **105**, 13 (1997).
3. M. Quilichini, P. Bernede, J. Lefevre, P. Schweiss, J. Phys. Cond. Matter **2**, 4543 (1990); M. Quilichini, V. Dvorak, P. Boutrouille, J. Phys. I France **1**, 1321 (1991).
4. A. Onodera, H. Yamashita, A. Molak, Ferroelectrics **172**, 319 (1995).
5. S. Constantinescu, S. Calogero, QCMP 172, QCPE Bull. **17**, 1 (1997).
6. R.M. Sternheimer, Phys. Rev. **80**, 102 (1950); **84**, 244 (1951); **95**, 736 (1954); **105**, 158 (1957); *Nuclear Quadrupole Coupling Constants*, in *NQR SPECTROSCOPY DATA* (Springer-Verlag, 1972).
7. D. Barb, S. Constantinescu, D. Tarina, J. Phys. I France **7**, 1701 (1997).
8. K.G. Wertheim, *Mössbauer effect, principles and applications* (Acad. Press, New York, 1964), p. 59.
9. I. Mikhail, K. Peters, Acta Cryst. B **35**, 1200 (1979).
10. R. Sommer, M. Maglione, J.J. Van Der Klink, Ferroelectrics **107**, 312 (1990).
11. R. Allman, G. Donney, Acta Cryst. B **27**, 1871 (1971).
12. S. Constantinescu, M.N. Grecu, D.C. Mateescu, D. Tarina, Rom. J. Phys. Suppl. **43**, 429 (1998).
13. B. Topic, U. Haeberlen, C. Blinc, S. Zumer, Phys. Rev. **43**, 91 (1991).
14. M.N. Grecu, V.V. Grecu, S.V. Nistor, M. Stefan, *Temperature dependence of Cu^{2+} EPR spectra in K_2ZnCl_4* in *Modern Aspects of Structure and Dynamic Investigation of Paramagnetic Systems by EPR*, p. 130, Third European ESR Meeting, Leipzig, Germany, 1997; 14th European Experimental NMR Conference, Bled, Slovenia, 10-15 May, 1998.